Electric/Hybrid Vehicle- Simulation Analysis

J. Knapik[1], R.E. Gallyamov[2], V.A. Ovchinnikov[2] , K.A. Volkova[3] , E.V. Avdeev[4]

[1]Laduga Automotive Engineering, Spring Valley Road 145, Westerville, United States, 43081
[2]Laduga Automotive Engineering, Frunze 14B, Togliatti, Russia, 445037
[3]Peter the Great St.Petersburg Polytechnic University, Polytehnicheskaia 29, St. Petersburg, Russia, 195251
[4]Samara National Research University, Moskovskoe Shosse 34A, Samara, Russia, 443086

Abstract. This report analyses computational research results of Electric Hybrid vehicle design and its main component characteristics. Two different versions are proposed and investigated. "Maximum allowable speed in each point" of the race track model (Le Mans race track) was tested. Conclusions on two hybrid car design packages; comparison and further research was completed.

Keywords: LMP1-H, packaging, maximum speed, best race time.

1. Introduction

Race vehicles/-race cars are for many manufacturers a great automotive system technology showcase. The report presents the results of computational research of Hybrid-Electric race vehicle packaging (using a LMP rule based car) and its main components characteristics.

2. Problem statement

The purpose of the learning task is to investigate effect of packaging, center of mass, car main units/ characteristics vs. “race lap” times. For a model of the track, the Le Mans GPS-track model [1] was used. The model has some detailed XYZ track information as seen in figure 1 & figure 2.

3. Drive cycle generation

First, the drive cycle was calculated to simulate the velocity of the race car at each location point on the Le Mans track. Track layout extraction for drive cycle generation is described in Section III-A.

Also, an estimate for the tire friction coefficients, which represent an important limitation of the maximum achievable speed in the drive cycle, is shown in Section III-B; the maximum car speed at each point was determined as target speed.

The model used for the drive cycle was based on a bicycle model, as the model considers transverse loads [4] [5]. Yet, the bicycle model has some flaws; it does not compute the car roll, suspension work, and the fact that the loads on both, the left and right half are different.

Figure 1. Le Mans GPS-track top view.

Figure 2. Le Mans GPS-track altitude.

3.1. Track layout

As pointed out in Section II, the track to be "drive" test samples are Le Mans, which layout is shown in figure 1. This GPS map was then converted to a list of radii by calculating the circum radius of every three points as shown in figure 3 using Python script [2]:

$$K = \sqrt{s(s-a)(s-b)(s-c)}\,, \tag{1}$$

where a, b, and c are the lengths (in m) of the sides of the triangle made of the three points and:

$$s = \frac{1}{2}(a+b+c)\,. \tag{2}$$

Finally, the radius R (in m) is calculated with:

$$R = \frac{abc}{4K}\,. \tag{3}$$

The radius calculated is said to be the radius of the middle point (i.e. point between sides: a and, b); the left- hand corners were defined to be positive and right- hand to be negative. The track layout, with all its parameters is shown in figure 4. Once the track layout was defined, the next step was to identify the tire friction coefficients, which determine the maximum speed achievable in the drive cycle.

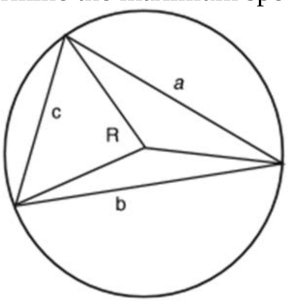

Figure 3. Circum radius R of three points constituting a triangle having lengths of a , b , and c .

3.2. Tire friction coefficients

Other necessary inputs used are the longitudinal and lateral tire friction coefficients. The Dunlop Formula 3 tire data was chosen for design; on which a linear and quadratic fits were created as shown in Figure 4. The difference between the linear and quadratic fit was negligible up to a normal force of 4,000 N (0.002 and 0.025 for the longitudinal and lateral friction coefficient, respectively).

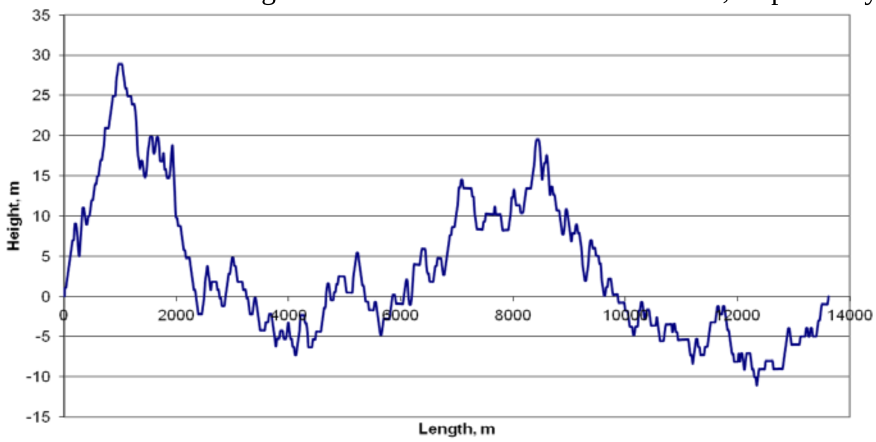

Figure 4. Drive cycle model – altitude.

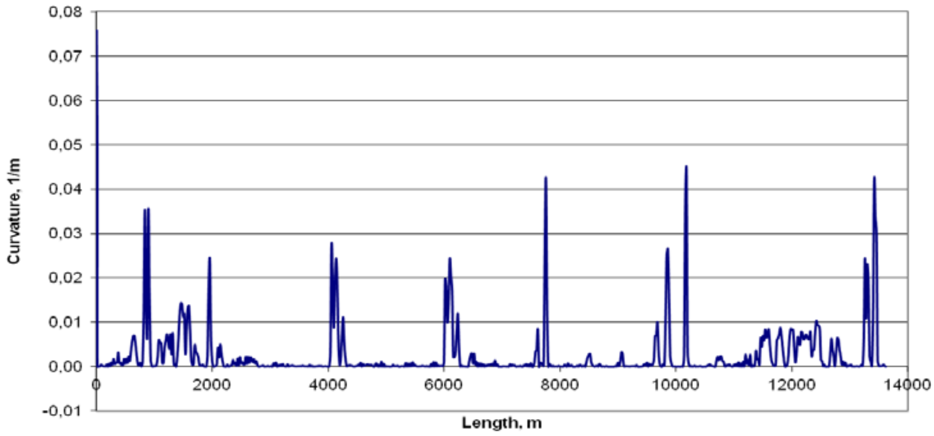

Figure 5. Drive cycle model – curvature.

Hence, the linear fit was chosen because of its simplicity. The friction coefficients in lateral and longitudinal directions are:

$$\mu_y = 1.8 + (-2.14) \cdot 10^{-6} \cdot F_z, \tag{4}$$

where F_z represents the normal force acting on the tire (in N). Once the tire friction coefficients were defined, the limits on the lateral force that could be generated by the tires could be determined.

3.3. Lateral force limit of the tires

The cornering velocity of a race car is fully defined by the maximum lateral force the tires can handle before losing grip. Therefore, tire friction coefficients are used to determine the maximum velocity as a function of the radius. This is done by limiting the centrifugal force, F_y (in N), to the maximum allowable lateral force on the tires, $F_{y,\max}$. The result of this step is shown in figure 5 above. Assuming steady state cornering, it can be written as:

$$F_y = \frac{m \cdot \vartheta^2}{abs(R)}, \tag{5}$$

where m (kg) is the mass of the race car and ϑ (m/s) is the velocity.

$$F_{y,\max} = F_{y,f} + F_{y,r} = F_y, \tag{6}$$

where $F_{y,f}$ and $F_{y,r}$ (N) are the maximum front and rear lateral forces (distributed equally over the two front/rear tires), given by:

$$F_{y,f} = \mu_{y,f}(F_{z,f}) \cdot F_{z,f}, \tag{7}$$

$$F_{y,r} = \mu_{y,r}(F_{z,r}) \cdot F_{z,r}. \tag{8}$$

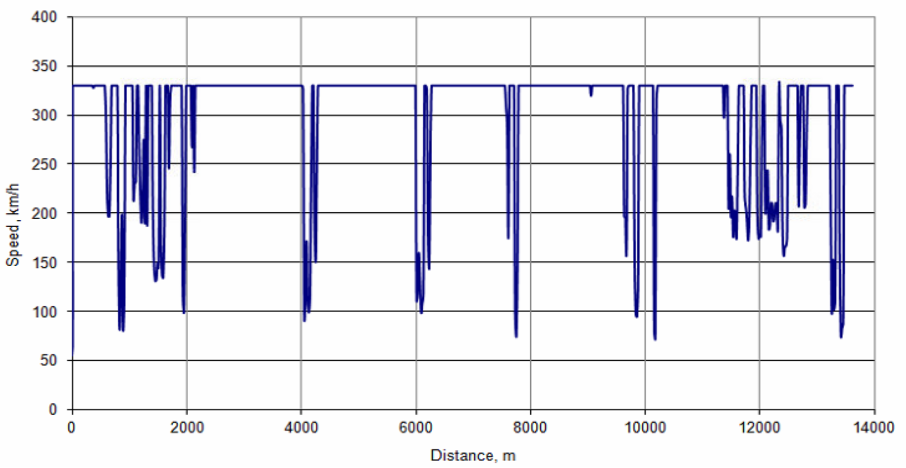

Figure 6. Maximum velocity due to the lateral tire limit.

Assuming a linear fit to the tire data, $\mu_{y,f}$ and $\mu_{y,r}$, the tires lateral friction coefficients can be expressed as:

$$\mu_{y,f} = c_3 + \frac{c_4}{2} \cdot F_{z,f}, \tag{9}$$

$$\mu_{y,r} = c_3 + \frac{c_4}{2} \cdot F_{z,r}, \tag{10}$$

Here c_4 coefficient is divided by two, to account for the fact that the tire data is for a single tire. For the normal forces $F_{z,f}$ and $E_{z,r}$ we can then write:

$$F_{z,f} = \frac{(m \cdot g + F_{down}(\nu)) \cdot L_r}{L}, \tag{11}$$

$$F_{z,r} = \frac{(m \cdot g + F_{down}(\nu)) \cdot L_f}{L}, \tag{12}$$

where m is the mass of the race car (kg), L is the length of the race car (m), and L_f and L_r are the lengths from the center of mass to the front and rear axle (m), respectively. F_{down} is the downforce of the race car (N) and is dependent on the speed based on equation below:

$$F_{down} = \frac{1}{2} C_{dd} \cdot \rho_{air} \cdot A_f \cdot c_d \cdot \upsilon^2, \tag{13}$$

where C_{dd} is the drag-to-downforce ratio, ρ_{air} is the air density (kg/m3), and c_d the drag coefficient. The drag coefficient is a measure of the drag-force created by the car's body, while the drag-to-downforce ratio is a relation between the drag force and the downforce generated by the car's body. A higher value of c_d could mean a lower straight-line acceleration, however, when combined with a higher value of C_{dd} this can lead to higher cornering speeds.

4. Mathematical model

Two hybrid /electric test packages are described in this section. On this stage the 1D model was used – the model takes into account longitudinal loads and computes the car roll.

Note: 1st - version's topology is shown in figure 7.

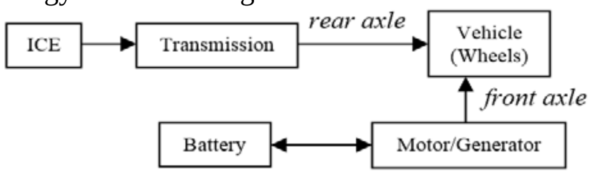

Figure 7. 1(single)-motor topology. ICE – Internal Combustion Engine.

2nd - car package is the same as the version "1" with an exception of additional Motor/Generator design. 2nd - car's version topology is shown in figure 8 below:

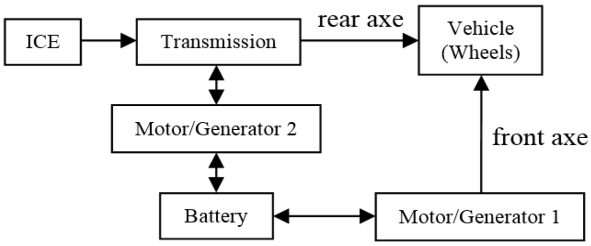

Figure 8. 2-motors topology. ICE – Internal Combustion Engine.

Car/ components masses are shown in table 1, below.

Table 1. Masses of main components.

Components	Masses, kg
Body	180
Engine	150
Driver	70
Clutch	20
Transmission	120
Motor-Generator rear	70
Motor-Generator front (only for 2-motors)	70
Batteries	100
Front wheels (including brakes and suspension)	100
Rear wheels (including brakes and suspension)	100
Fuel tank (including fuel)	50
Engine radiator	20

*Total mass of a single motor vehicle is 980 kg & total mass of 2-motor optional vehicle is 1050 kg.

To simulate car movement along the track, it is necessary to determine the location of car's center of mass. The optimal car components layout should satisfy two basic requirements: total center of mass should be as low as possible, the center of mass should be in the middle - at the same distance from the front and rear axle of the car. Taking these two requirements into account and using our "Le Mans Prototype (see figure 9) model, the; centers of mass were calculated and presented respectively in table 2, table 3.

The coordinates of the center of mass are determined relative to rotation center of the rear axle.

Centers of masses of car components and total center of mass: 1-motor version are shown in table 2.

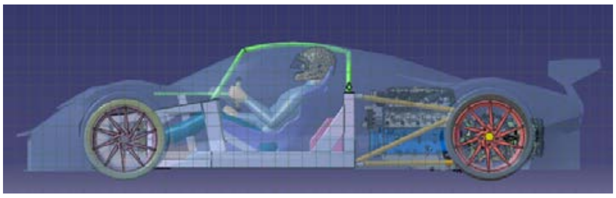

Figure 9. Le Mans Prototype car model used for layout analysis[7].

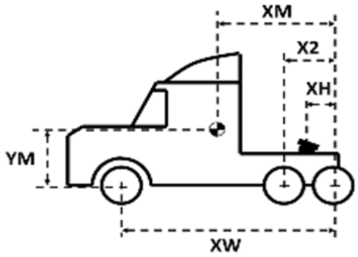

Figure 10. XM, YM distance determination, relative to rotation center of the rear axle.

Table 2. Centers of masses of components for 1-motor version.

Components	XM, mm	YM, mm
Body	1500	100
Engine	700	0
Driver	1800	0
Clutch	440	0
Transmission	-150	0
Motor-Generator rear	270	0
Batteries	1500	-100
Front wheels (including brakes and suspension)	3005	0
Rear wheels (including brakes and suspension)	0	0
Fuel tank (including fuel)	1360	-70
Engine radiator	3200	100
Total	1043	6

Centers of masses of car components and total center of mass: 2-motor version are shown in table 3.

Table 3. Centers of masses of components for 2-motor version.

Components	XM, mm	YM, mm
Body	1500	100
Engine	700	0
Driver	1800	0
Clutch	440	0
Transmission	-150	0
Motor-Generator 1 rear	270	0
Motor-Generator 2 front	270	3000
Batteries	1500	-100
Front wheels (including brakes and suspension)	3005	0
Rear wheels (including brakes and suspension)	0	0
Fuel tank (including fuel)	1360	-70
Engine radiator	3200	100
Total	1241	6

5. Modeling and analysis

For Single & 15 lap "race" the following results were recorded (see table 4).

Table 4. Lap time comparison

Car version	1lap Time, s	15 laps Time, s
1-motor	288.5	4243.3
2-motors	289.2	4252.3

As observed both design options showed the lap times that are "too slow" compared to lap times capable by "real race cars" on the same track [3]. One of the main reasons is the discrepancy between engine and electric motor rotational frequencies. The engine spec provided for this project is the "most powerful" on high rotational frequencies 10000-12000 RPM (see figure 11), however, electric motors are effective on frequencies around 1500-2000 RPM (see figure 12). Overall, the project was constructive in exploring a hybrid electric car behavior, and as for the efficiency /frequency issue, that can be solved by 'more "suitable transmission ratio selection. In the end, a comparative qualitative analysis between both suggested samples, (single motor and 2-motor designs) was completed as intended.

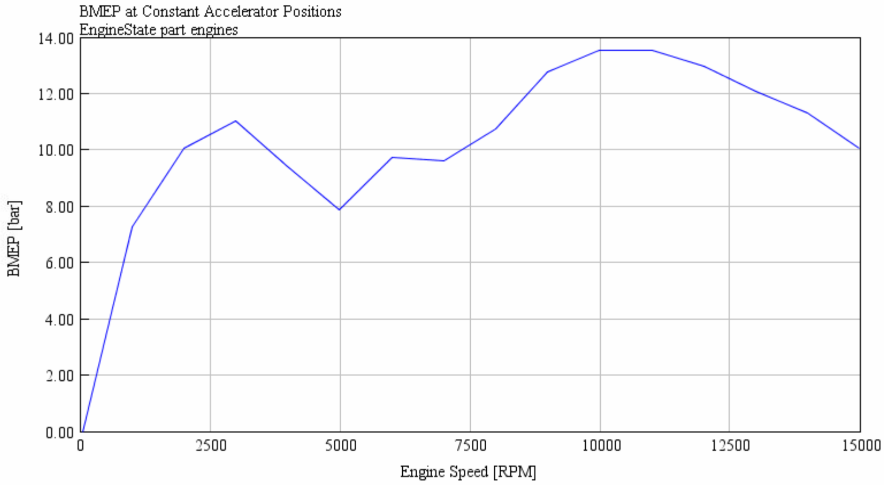

Figure 11. Brake mean effective pressure of Engine, bar.

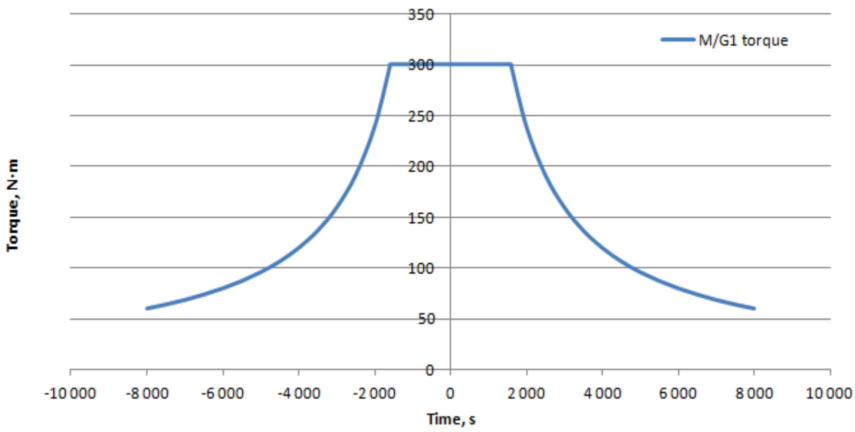

Figure 12. Motor/Generator max torque.

The target and actual speed for 1-motor and 2-motor versions are shown in figure 13, figure 14 accordingly. Please note that target speeds are different for each package because target speed calculation takes into account the mass of the car, which is different for single (1) and 2-motor vehicle.

Use of KERS (Kinetic Energy Recovery System) in the project was driven by a few factors, mainly by the fact that most of modern race vehicles are equipped with such system and, secondary by KERS' action impact, if any, on both designed versions tested. The data for the unit was used from article by Flybrid Systems (*The Flybrid KERS was used first time ever in 24-hrs race by a hybrid car in 2011 [6]).

KERS as implemented in the project works in 3 modes:

1. No braking. KERS is off.
2. Car braking, the Motor/Generator braking power is sufficient; greater than the required requested braking power. Car uses only Motor/Generator for braking and generates electric energy, which charges battery.
3. Car braking, the Motor/Generator braking power is insufficient; smaller than the required requested braking power. Car uses Motor/Generator and mechanical brakes for braking.

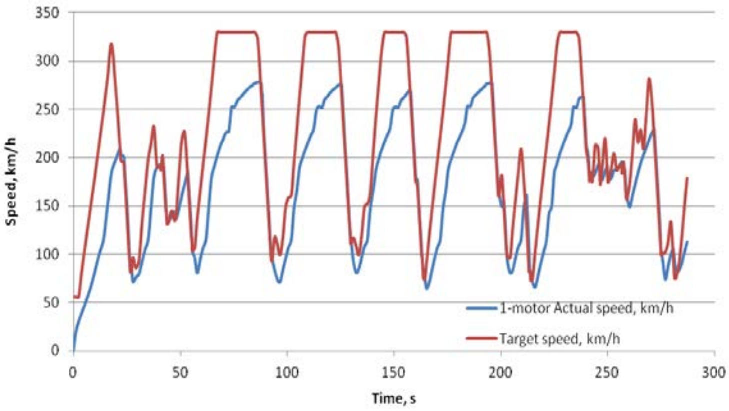

Figure 13. Target and actual speed : 1-motor version(1 lap).

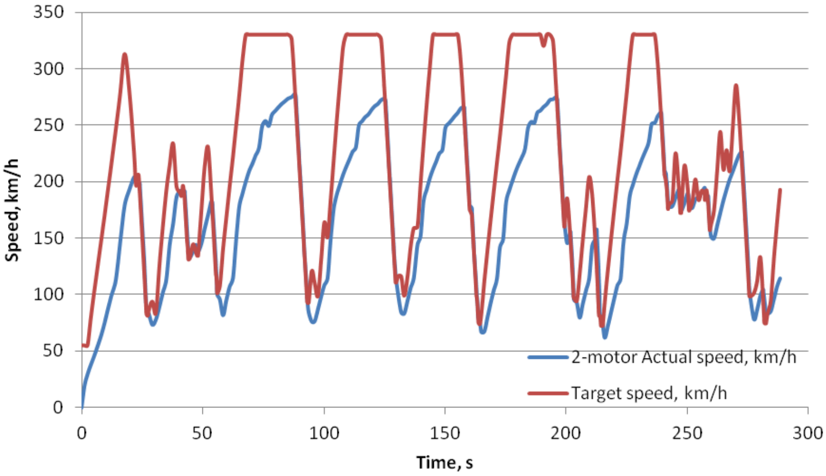

Figure 14. Target and actual speed : 2-motor version (1 lap).

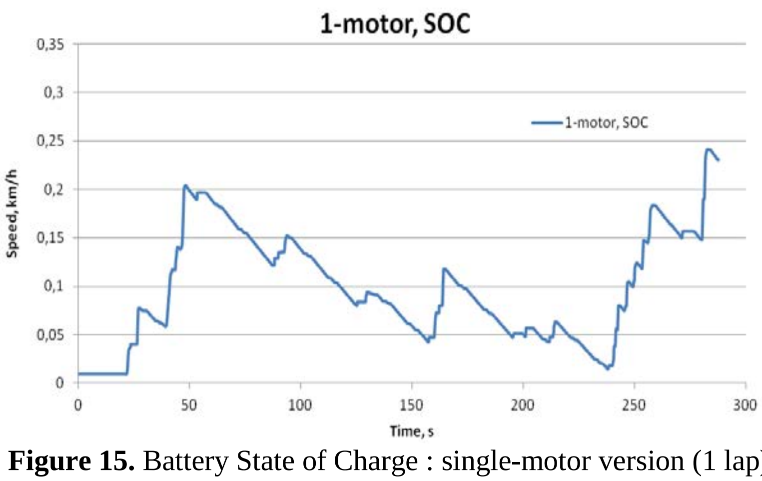

Figure 15. Battery State of Charge : single-motor version (1 lap).

As shown in both figures - (figure 15 and figure. 16) - the Battery State of Charge charts the in 2-motor design option equipped with KERS works more efficiently. Additional Motor/Generator allows storing more energy during braking since the energy is received from both axes. This “allows” to reduce battery capacity needs by 70% less from the present state.

Note that, torque on Motor/Generator is shown in figure 17 and figure 18. *Positive torque corresponds to the energy consumption, motor mode. Negative torque corresponds to energy generation – “generator mode”.

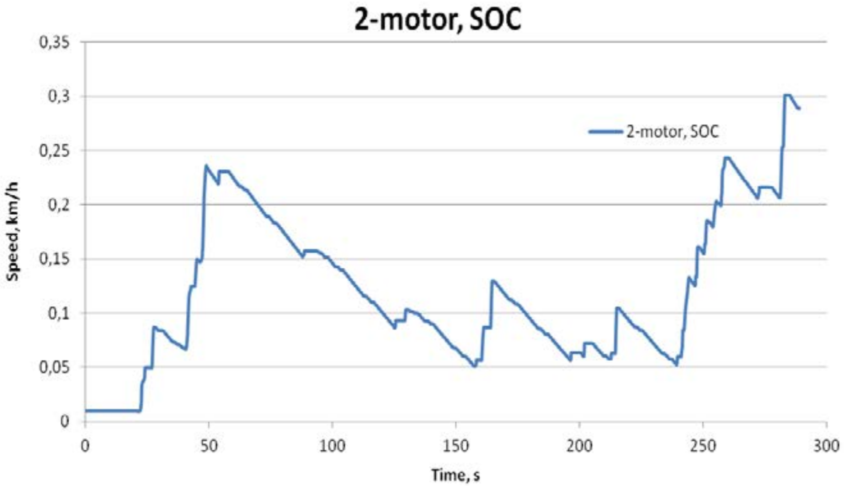

Figure 16. Battery State of Charge: 2-motor version (1 lap).

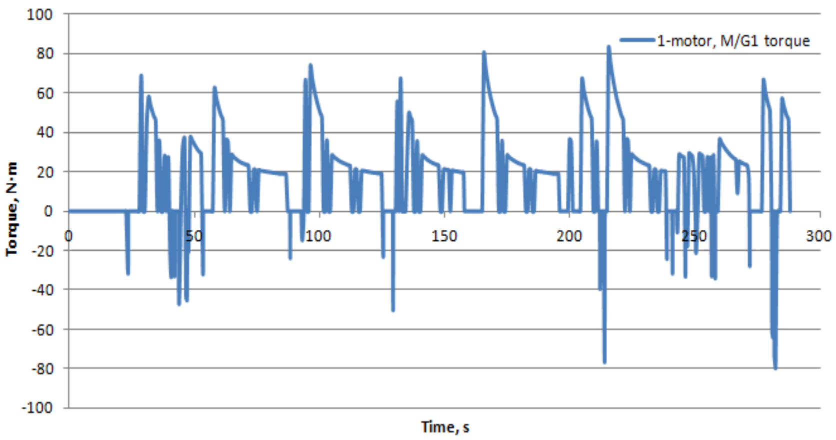

Figure 17. Torque on Motor/Generator: single-motor version (1 lap).

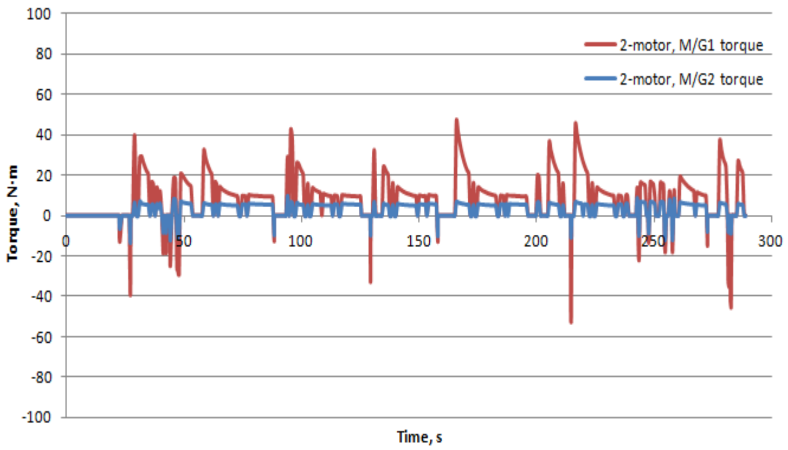

Figure 18. Torque on Motor/Generators: 2-motor version (1 lap).

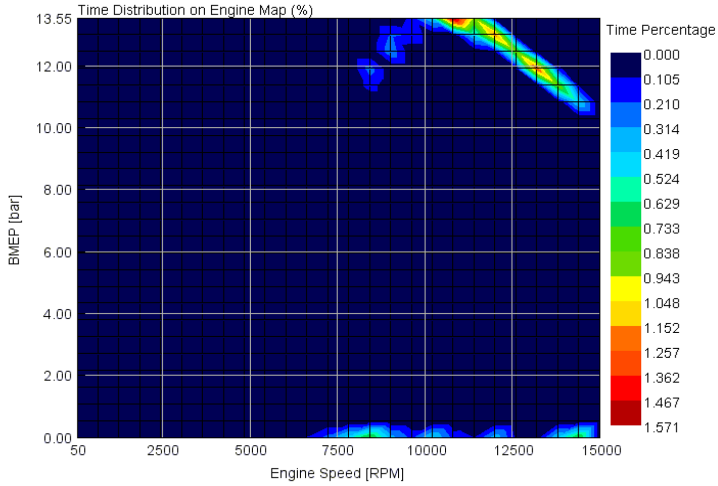

Figure 19. Time Distribution on Engine Map for 2-motor version (1 lap).

6. Conclusion

As mentioned earlier, the engine efficiency can be increased by transmission ratio optimization. In current spec the engine runs at high rotational frequencies (see figure 19), while the Motor/Generator is effective at low frequencies.

Despite the ‘slow’ lap times (288.4 s for 1-motor and 289.2 s for 2-motor configuration) caused by a discrepancy of both, engine and motor frequencies; the study of behavior of two hybrid powertrain configurations was moderate success. Additional efforts and time may be needed in fine- tuning and testing these configurations and components such as engine, transmission or the battery. For example, the 2-motor - KERS design option with a new, lighter battery of much lower capacity that was initially used would mitigate overall vehicle mass ,hence could improve the lap speeds.

In conclusion, the 2-motor design option showed more efficiency of KERS system, but with the single-motor design lap times were improved caused by reduced vehicle mass.

7. References

[1] Jacob, J. In Motion: Hybrid race car, beating F1 at LeMans / J.A. Colin, H. Montemayor, D. Sepac, H.D. Trinh, S.F. Voorderhake, P. Zidkova, J.J.H. Paulides, A. Borisavljevic, E.A. Lomonova Ecological // Vehicles and Renewable Energies (EVER), 2013 8th International Conference and Exhibition, 2013. DOI: 10.1109/EVER.2013.6521638.

[2] Car tour Arnage SARTHE GPS-map [Electronic resource]. – Access mode: https://www.gpsies.com/map.do;jsessionid=057124D22998D971691C2FFC51B3AE56.fe1?fileId=kvuebdwexgpvgmcr (16.11.2017).

[3] Wikipedia: List of 24 hours of Le Mans records [Electronic resource]. – Access mode: https://en.wikipedia.org/wiki/List_of_24_hours_of_Le_Mans_records (16.11.2017).

[4] Kong, J. Kinematic and dynamic vehicle models for autonomous driving control design / J. Kong, M. Pfeiffer, G. Schildbach, F. Borrelli // Intelligent Vehicles Symposium (IV), 2015. DOI: 10.1109/IVS.2015.7225830.

[5] Mod-01 Lec-18 Lateral Dynamics – Bicycle Model [Electronic resource]. – Access mode: https://www.youtube.com/watch?v=umkWxXgQelk (16.11.2017).

[6] Milton, J. Flywheel hybrid systems in motorsport - Flybrid Systems LLC / J. Milton // [Electronic resource]. – Access mode: http://www.torotrak.com (16.11.2017).

[7] Lateral Vehicle Dynamics [Electronic resource]. – Access mode: http://users.sussex.ac.uk/~tafb8/mas/MAS_03a_LateralVehicleDynamics.pdf (16.11.2017).

[8] LMP1 Race Car - Le Mans 3D model [Electronic resource]. – Access mode: https://3dwarehouse.sketchup.com/model/u662155db-f89b-4633-9f0d-94deb6bd54be/LMP1-Race-Car-Le-Mans (16.11.2017).